

High contribution of anthropogenic combustion sources to atmospheric inorganic reactive nitrogen in South China evidenced by isotopes

Tingting Li^{1,2,4}, Jun Li^{*1,2}, Zeyu Sun^{3,4}, Hongxing Jiang¹, Chongguo Tian³, Gan Zhang^{1,2}

¹State Key Laboratory of Organic Geochemistry and Guangdong province Key Laboratory of Environmental Protection and Resources Utilization, Guangdong-Hong Kong-Macao Joint Laboratory for Environmental Pollution and Control, Guangzhou Institute of Geochemistry, Chinese Academy of Sciences, Guangzhou, 510640, China

²CAS Center for Excellence in Deep Earth Science, Guangzhou 510640, P. R. China

³Yantai Institute of Coastal Zone Research, Chinese Academy of Sciences, Yantai 264003, P. R. China

⁴University of Chinese Academy of Sciences, Beijing 100049, P. R. China

*Correspondence to: Jun Li (junli@gig.ac.cn)

Abstract: Due to the intense release of reactive nitrogen (Nr) from anthropogenic activity, the source layout of atmospheric nitrogen aerosol has changed. The inorganic nitrogen (NH_4^+ and NO_3^-) was essential part of atmospheric nitrogen aerosol and accounted for 69%. To comprehensively clarify the level, sources, and environmental fate of NH_4^+ and NO_3^- , their concentrations and stable isotopes ($\delta^{15}\text{N}$) in fine particulate matters ($\text{PM}_{2.5}$) were measured in a subtropical megacity of South China. N- NH_4^+ and N- NO_3^- contributed 45.8% and 23.2% to total nitrogen (TN), respectively. The source contributions of NH_4^+ and NO_3^- were estimated by $\delta^{15}\text{N}$, which suggested that anthropogenic combustion activities including coal combustion, biomass burning, and vehicles were dominant sources. Especially, biomass burning was the predominant source of NH_4^+ (27.9%). Whereas, coal combustion was the dominant source of NO_3^- (40.4%). This study emphasized the substantial impacts of human activities on inorganic Nr. With the rapid development of industry and transportation, nitrogen emissions will be even higher. The promotion of clean energy and efficient use of biomass would help reduce nitrogen emissions and alleviate air pollution.

30 1. Introduction

31 Nitrogenous aerosols are ubiquitous in environment and play an important role as
32 nutrients in ecosystems(Bhattarai et al., 2019). With the massive combustion of fossil fuels and
33 the development of livestock, the proportion of TN in particulate matter (PM) ranges from 1.2%
34 to 17.0% and has shown a rapid increase in the last few decades(Bhattarai et al., 2019;
35 Galloway et al., 2004; Holland et al., 1999). Mostly nitrogenous aerosols formed from
36 atmospheric Nr will be deposited into terrestrial and aquatic ecosystems(Huang et al., 2015).
37 Excessive external nitrogen deposition accelerates nitrogen loss in soil, decreases species
38 diversity, disturbs terrestrial ecosystems, and leads to eutrophication in aquatic
39 ecosystems(Breemen, 2002; Wedin and Tilman, 1996; Yang et al., 2015). Furthermore,
40 nitrogenous aerosols have adverse impacts on the climate, air quality, and human
41 health(Bhattarai et al., 2019; Song et al., 2021).

42 N-NO₃⁻ and N-NH₄⁺ as inorganic Nr are dominant species in the deposition of
43 nitrogen(Zhu et al., 2015). N-NH₄⁺ was the highest in nitrogen deposition, and NH₄⁺ was
44 gradually considered to be an important component of secondary inorganic aerosols (SIA)(Sun
45 et al., 2021). NH₃, the precursor of NH₄⁺, is a vital atmospheric alkaline gas, which can
46 participate in nucleation to promote ~~the~~ new particles generation, and can react with acid gas
47 to produce ammonium sulfate and ammonium nitrate(Dunne et al., 2016; Fu et al., 2017). The
48 excessive NH₃ emission from anthropogenic sources will partially offset the benefits of
49 reducing SO₂ and NO_x and trigger urban haze in China(Sun et al., 2021; Meng et al., 2018;
50 Pan et al., 2018a). In many urban environments, NO₃⁻ has replaced sulfate as the component
51 with the highest proportion in SIA. NO_x, precursors of NO₃⁻, are also closely related to the
52 formation of atmospheric oxidants and exert important effects on atmospheric oxidation. In
53 addition, NH₄NO₃ in PM plays an increasingly important role in promoting the formation of
54 sulfate and organic matter, and has profound effect on the physical and chemical properties of
55 PM(Liu et al., 2021; Liu et al., 2020; Hodas et al., 2014). Therefore, to mitigate ~~the~~ nitrogen
56 deposition and air pollution, the control of NH₄⁺ (NH₃) and NO₃⁻ (NO_x) should not be neglected.

57 Considerable efforts have been made to comprehensively ly understand the budget of
58 atmospheric NH₄⁺ and NO₃⁻. δ¹⁵N is effective to quantify sources contribution of nitrogenous

59 species(Elliott et al., 2007). The anthropogenic combustion sources (combustion of coal,
60 biomass, and gasoline) play a key role in the emission of NO_3^- (NO_x) in many regions of China
61 suggested by $\delta^{15}\text{N}$ (Zong et al., 2020), which also have large effects on NH_3 (Chen et al., 2022b).
62 NH_3 is released by agricultural sources (agricultural activity and livestock) and non-agricultural
63 sources (fossil fuel combustion and vehicle)(Bhattarai et al., 2019). ~~Previous-A previous~~ study
64 showed that agricultural source was the dominant source (80%-90%) of NH_3 in China(Kang et
65 al., 2016). However, NH_3 emissions from agricultural source have been reduced due to
66 intensive farming and efficient fertilization(Wang et al., 2022). ~~Combustion sources were~~
67 ~~gradually becoming dominant sources of urban NH_3 in recent years verified by the methods of~~
68 ~~emission inventory and $\delta^{15}\text{N}$ (Xiao et al., 2020; Meng et al., 2017). Especially, the incomplete~~
69 ~~burning of biomass leads to massive NH_3 emission and is gradually to be the second largest~~
70 ~~non-agricultural source of NH_3 (Yu et al., 2020), which may be responsible for the lag of the~~
71 ~~decline in air pollutants deposition behind the reduction in emission of precursors(Zhao et al.,~~
72 ~~2022b).The incomplete burning of biomass leads to massive NH_3 emissions and is gradually~~
73 ~~to be the second largest non-agricultural source of NH_3 (Yu et al., 2020), which may be~~
74 ~~responsible for the lag of the decline in air pollutants deposition behind the reduction in~~
75 ~~emission of precursors(Zhao et al., 2022b). Biomass burning in the suburbs also has a potential~~
76 ~~impact on urban NH_3 (Xiao et al., 2020). As for urban NH_3 , combustion sources (including coal~~
77 ~~combustion, vehicles emission, and biomass burning) were gradually becoming dominant~~
78 ~~sources in recent years verified by $\delta^{15}\text{N-NH}_x$ ($\text{NH}_3+\text{NH}_4^+$)(Xiao et al., 2020; Pan et al., 2018b).~~
79 In addition, the super clean emission of coal-fired power plant and strict emission standards of
80 vehicles will change the source layout of NH_4^+ and NO_3^- . Selective catalytic reduction
81 technology equipped with vehicles and industrial boiler reduces NO_x but increases NH_3
82 emissions(Meng et al., 2017; Pan et al., 2016). The occurrence of haze in North China was
83 closely related to NH_3 emissions from combustion sources(Pan et al., 2018a; Pan et al., 2018b).
84 NH_4^+ and NO_3^- are the main components of SIA and play a vital role in the formation of
85 secondary aerosol(Meng et al., 2017), so it is necessary to revisit their sources.

86 NH_3 emissions from densely populated subtropical areas increased rapidly with the high
87 development of industry and transportation(Wang et al., 2013). Guangzhou is the core megacity
88 in the South subtropical region of China, where the atmospheric environment is complex and

89 the atmospheric oxidation level is high(Tan et al., 2019). The high emissions of inorganic
90 nitrogen ~~form~~from anthropogenic combustion sources have serious and profound impacts on
91 the environment. In this study, we aimed to comprehensivelyly clarify the level of inorganic Nr
92 and revisit the source layout of atmospheric inorganic Nr.

93 2. Experimental and theoretical methods

94 2.1. Sampling and Chemical concentration analysis

95 PM_{2.5} samples (n=66) were collected from May 2017 to June 2018 in Guangzhou
96 (23.13°N, 113.27°E). Details of sample collection can be found in our previous study(Jiang et
97 al., 2021a). The chemical components including water-soluble ions (i.e., NH₄⁺, K⁺, Na⁺, Ca²⁺,
98 Mg²⁺, Cl⁻, NO₃⁻, and SO₄²⁻), organic carbon (OC), element carbon (EC), and organic molecular
99 markers (e.g., levoglucosan) were analyzed in our previous studies (**SI Text S1**)(Jiang et al.,
100 2021a; Jiang et al., 2021b). Moreover, meteorological parameters (temperature, relative
101 humidity (RH), atmosphere pressure, and wind speed) and the concentration of trace gases (CO,
102 SO₂, NO, NO₂, and O₃) were acquired by online instruments (details shown in **SI Text S1**). A
103 circular punch (r=1cm) of the sample filter was wrapped in a tin boat and then measured in an
104 elemental analyzer to determine the concentrations of TN.

105 2.2. Isotope analysis

106 The δ¹⁵N-NO₃⁻ and δ¹⁸O-NO₃⁻ values in PM_{2.5} ~~was~~were analyzed by methods of nitrous
107 oxide (N₂O), which was described in previous study in detail(Zong et al., 2017). Briefly, NO₃⁻
108 was reduced to NO₂⁻ using cadmium powder and imidazole solution, and N₂O was made by
109 adding NaN₃ to NO₂⁻ solution. The production of 75nmol N₂O gas was needed to measure. The
110 N₂O gas produced by above processes was measured by MAT253 stable isotope mass
111 spectrometer. The values of δ¹⁸O and δ¹⁵N were expressed in per mil (‰) shown in Eq. (1) and
112 (2), relative to the international oxygen and nitrogen isotope standard, respectively.

$$113 \delta^{15}\text{N} = \left[\frac{(^{15}\text{N}/^{14}\text{N})_{\text{sample}}}{(^{15}\text{N}/^{14}\text{N})_{\text{standard}}} - 1 \right] * 1000 \quad (1)$$

$$114 \delta^{18}\text{O} = \left[\frac{(^{18}\text{O}/^{16}\text{O})_{\text{sample}}}{(^{18}\text{O}/^{16}\text{O})_{\text{standard}}} - 1 \right] * 1000 \quad (2)$$

115 The δ¹⁵N-NH₄⁺ was measured by methods of hypobromite oxidation coupled with

116 reduction of hydroxylamine hydrochloride(Sun et al., 2021). Briefly, NH_4^+ was oxidated to
117 NO_2^- using alkaline hypobromite (BrO^-), and N_2O was made by adding sodium arsenite and
118 hydrochloric acid to NO_2^- solution. The production of 120 nmol N_2O gas was needed to
119 measure. The N_2O gas produced by above processes was measured by MAT253 stable isotope
120 mass spectrometer. The values of $\delta^{15}\text{N}$ were expressed in per mil (‰), Eq. (1). To ensure the
121 stability of the instrument, standard samples were tested for every ten samples. The standard
122 deviation of replicates was generally less than 0.4‰, 0.8‰, and 0.5‰ for $\delta^{15}\text{N}-\text{NO}_3^-$, $\delta^{18}\text{O}-$
123 NO_3^- , and $\delta^{15}\text{N}-\text{NH}_4^+$, respectively. The instrumental values of $\delta^{15}\text{N}-\text{NO}_3^-$ and $\delta^{18}\text{O}-\text{NO}_3^-$ were
124 corrected by multi-point correction ($\delta^{18}\text{O}$ $r^2=0.99$, $\delta^{15}\text{N}$ $r^2=0.999$) based on international
125 standards (IAEA-NO-3, USGS32, USGS34, and USGS35). The measured values of $\delta^{15}\text{N}-\text{NH}_4^+$
126 were also corrected by multi-point correction ($r^2=0.999$) based on international standards
127 (IAEA-N1, USGS25, and USGS26). In addition, ^7Be and ^{210}Pb were acquired and details were
128 shown in **SI Text S1**.

129 **2.3. IsoSource and Bayesian mixing and IsoSource model**

130 **IsoSource model.** IsoSource model was released by Environmental Protection Agency
131 (EPA), could calculate ranges of source contributions to a mixture based on conservation of
132 isotopic mass when number of sources is too large to permit a unique solution and provide the
133 distribution of source proportions (Phillips et al., 2005). IsoSource model coupled with $\delta^{15}\text{N}-$
134 NH_3 of atmospheric initial and potential sources (shown in Table 1) were applied to quantify
135 the contribution of various sources to NH_3 . Nitrogen fertilizers application, livestock, human
136 waste, biomass burning, coal combustion, and vehicles were considered as sources of NH_3 in
137 this study, details shown in **SI Text S2**. Atmospheric initial $\delta^{15}\text{N}-\text{NH}_3$ was calculated by
138 following Eq. (3).

$$139 \quad \delta^{15}\text{N}-\text{NH}_{3\text{-initial}} = \delta^{15}\text{N}-\text{NH}_4^+ - \varepsilon(\text{NH}_4^+-\text{NH}_3) \times (1 - f) \quad (3)$$

140 Where, $\delta^{15}\text{N}-\text{NH}_4^+$ and $\delta^{15}\text{N}-\text{NH}_{3\text{-initial}}$ represent the $\delta^{15}\text{N}$ of particulate NH_4^+ and
141 atmospheric initial NH_3 , respectively. $\varepsilon(\text{NH}_4^+-\text{NH}_3)$ represents the isotope fractionation factor
142 in the gaseous NH_3 conversion to particulate NH_4^+ in the atmosphere. The f value represents
143 the proportion of the initial NH_3 converted to NH_4^+ , referring to NH_3 and NH_4^+ observed in
144 Guangzhou (Liao et al., 2014).

The $\epsilon(\text{NH}_4^+-\text{NH}_3)$ value is temperature dependent(Huang et al., 2019), which can be deduced from(Urey, 1947), as shown in Eq. (4). The atmospheric average temperature was 24.5°C in our sampling period, and the corresponding $\epsilon(\text{NH}_4^+-\text{NH}_3)$ value was 34.2‰ calculated by Eq. (4). In addition, the $\epsilon(\text{NH}_4^+-\text{NH}_3)$ in Guangzhou was estimated to be 32.4‰ according to Eq. (8). Eq. (8) was deduced by Eq. (5-7). According to Eq. (8), a linear fitting equation was observed between $f\text{NH}_4^+$ and $\delta^{15}\text{N}-\text{NH}_4^+$ (Fig. S1), and the absolute value of the slope (32.4‰) was equal to $\epsilon(\text{NH}_4^+-\text{NH}_3)$. The $\epsilon(\text{NH}_4^+-\text{NH}_3)$ average of the two methods (34.2‰ and 32.4‰) was 33.3‰ and approximated to the experimental isotope enrichment factor (33‰)(Heaton et al., 1997). Therefore, 33‰ was used for deducing the $\delta^{15}\text{N}$ of the initial NH_3 .

$$\epsilon_{(\text{NH}_4^+_{-}\text{NH}_3)} = 12.4678 * \frac{1000}{T+273.15} - 7.6694 \quad (4)$$

$$\delta^{15}\text{N}-\text{NH}_4^+ - \delta^{15}\text{N}-\text{NH}_3 = \epsilon_{(\text{NH}_4^+_{-}\text{NH}_3)} \quad (5)$$

$$f\text{NH}_4^+ + f\text{NH}_3 = 1 \quad (6)$$

$$\delta^{15}\text{N}-\text{NH}_4^+ * f\text{NH}_4^+ + (\delta^{15}\text{N}-\text{NH}_4^+ - \epsilon_{(\text{NH}_4^+_{-}\text{NH}_3)}) * (1 - f\text{NH}_4^+) = \delta^{15}\text{N} \quad (7)$$

$$\delta^{15}\text{N}-\text{NH}_4^+ = -\epsilon_{(\text{NH}_4^+_{-}\text{NH}_3)} * f\text{NH}_4^+ + (\delta^{15}\text{N} + \epsilon_{(\text{NH}_4^+_{-}\text{NH}_3)}) \quad (8)$$

Where, T represents the atmospheric temperature (°C). $\delta^{15}\text{N}-\text{NH}_4^+$ and $\delta^{15}\text{N}-\text{NH}_3$ represent the $\delta^{15}\text{N}$ of particulate NH_4^+ and atmospheric NH_3 , respectively. $\delta^{15}\text{N}$ represents the sum of $\delta^{15}\text{N}-\text{NH}_4^+$ and $\delta^{15}\text{N}-\text{NH}_3$. $f\text{NH}_3$ and $f\text{NH}_4^+$ represent the proportion of atmospheric NH_3 and particulate NH_4^+ , respectively.

Bayesian mixing model. $\delta^{15}\text{N}$ were used for tracing source based on conservation of isotopic mass. Bayesian mixing model improved upon linear mixing models by explicitly considering uncertainty in prior information and isotopic equilibrium fractionation. Recently, Bayesian mixing model was applied to trace the sources of atmospheric pollutants(Zong et al., 2017; Zong et al., 2020). The model coupled with $\delta^{15}\text{N}-\text{NO}_3^-$ and $\delta^{18}\text{O}-\text{NO}_3^-$ were used to identify the formation process and quantify the sources contribution of NO_3^- .

In Central Pearl River Delta (PRD), NO_3^- formed through $\cdot\text{OH}$ and N_2O_5 pathways contributed to 94% simulated by CAMQ model (Qu et al., 2021). In this study, only $\cdot\text{OH}$ and N_2O_5 formation pathways were considered. Details of NO_3^- formation pathway were also shown in SI Text S2. The atmospheric $\delta^{18}\text{O}-\text{NO}_3^-$ can be expressed by Eq. (9). The $[\delta^{18}\text{O}-$

173 HNO₃]_{OH} can be further expressed by Eq. (10) assuming no kinetic isotope fractionation
 174 (Walters and Michalski, 2016). And [¹⁸O-HNO₃]_{H₂O} can be estimated by Eq. (11) (Walters and
 175 Michalski, 2016). The δ¹⁸O values in tropospheric H₂O, NO_x, O₃, and OH were within a certain
 176 range. The tropospheric δ¹⁸O-H₂O, δ¹⁸O-NO_x, δ¹⁸O-O₃, and δ¹⁸O-OH ranged from -25‰ to
 177 0‰(Baskaran et al., 2011; Walters and Michalski, 2016), 112‰ to 122‰ (Michalski et al.,
 178 2014; Walters and Michalski, 2016), 90‰ to 122‰, and -15‰ to 0‰, respectively(Fang et al.,
 179 2011; Johnston and Thiemens, 1997). Therefore, the γ (the contribution of ·OH formation
 180 pathway) can be estimated by fNO₂ and oxygen isotope fractionation i.e., αNO₂/NO, αOH/H₂O,
 181 and αN₂O₅/NO₂. The oxygen isotope fractionations are temperature dependent and can be
 182 estimated by Eq. (13) and **Table S1**. The fNO₂ varied from 0.20 to 0.95(Zong et al., 2017;
 183 Walters et al., 2016). Based on δ¹⁸O-NO₃⁻, δ¹⁸O-H₂O, δ¹⁸O-NO_x, δ¹⁸O-O₃, and temperature
 184 (Eq. (9-13)), γ (maximum γ and minimum γ) was estimated by Monte Carlo simulation nested
 185 in Bayesian mixing model (Zong et al., 2017). Assuming no kinetic isotope fractionation, the
 186 nitrogen isotope fractionation value in the formation process of NO₃⁻ (εN) was calculated by
 187 Eq. (13-16) combined with γ and temperature (Zong et al., 2017; Walters and Michalski, 2016;
 188 Walters et al., 2016). The εN value in our sampling period was 5.1±2.5‰, which was
 189 comparable to that in Beijing(average 6.5‰)(Fan et al., 2020). The contributions of different
 190 sources to atmospheric NO_x were quantified by Bayesian mixing model coupled with εN, δ¹⁵N-
 191 atmospheric-NO₃⁻, and δ¹⁵N-NO_x endmembers shown in **Table 1**. We considered coal
 192 combustion, mobile traffic sources, biomass burning, and soil microbial process as dominant
 193 atmospheric NO_x sources in Guangzhou, details shown in **SI Text S2**. The specific details of
 194 Bayesian mixing model were reported by our previous studies(Zong et al., 2017; Zong et al.,
 195 2020).

$$196 \delta^{18}\text{O}-\text{NO}_3^- = \gamma \times [\delta^{18}\text{O}-\text{NO}_3^-]_{\text{OH}} + (1 - \gamma) \times [\delta^{18}\text{O}-\text{NO}_3^-]_{\text{H}_2\text{O}} = \gamma \times [\delta^{18}\text{O}-\text{HNO}_3]_{\text{OH}} +$$

$$197 (1 - \gamma) \times [\delta^{18}\text{O}-\text{HNO}_3]_{\text{H}_2\text{O}} \quad (9)$$

$$198 [\delta^{18}\text{O}-\text{HNO}_3]_{\text{OH}} = \frac{2}{3} [(\delta^{18}\text{O}-\text{NO}_2)]_{\text{OH}} + \frac{1}{3} [\delta^{18}\text{O}-\text{OH}]_{\text{OH}} = \frac{2}{3} \left[\frac{1000 \times ({}^{18}\alpha_{\text{NO}_2/\text{NO}} - 1)(1 - f_{\text{NO}_2})}{(1 - f_{\text{NO}_2}) + ({}^{18}\alpha_{\text{NO}_2/\text{NO}} \times f_{\text{NO}_2})} + \right.$$

$$199 \left. [\delta^{18}\text{O}-\text{NO}_x] \right] + \frac{1}{3} [(\delta^{18}\text{O}-\text{H}_2\text{O}) + 1000 \times ({}^{18}\alpha_{\text{OH}/\text{H}_2\text{O}} - 1)] \quad (10)$$

$$[\delta^{18}\text{O}-\text{HNO}_3]_{\text{H}_2\text{O}} = \frac{5}{6}(\delta^{18}\text{O}-\text{N}_2\text{O}_5) + \frac{1}{6}(\delta^{18}\text{O}-\text{H}_2\text{O}) \quad (11)$$

$$\delta^{18}\text{O}-\text{N}_2\text{O}_5 = \delta^{18}\text{O}-\text{NO}_2 + 1000 \times (\alpha_{\text{N}_2\text{O}_5/\text{NO}_2} - 1) \quad (12)$$

$$1000(\alpha_{\text{X}/\text{Y}} - 1) = \frac{\text{A}}{\text{T}^4} \times 10^{10} + \frac{\text{B}}{\text{T}^3} \times 10^8 + \frac{\text{C}}{\text{T}^2} \times 10^6 + \frac{\text{D}}{\text{T}} \times 10^4 \quad (13)$$

$$\begin{aligned} \varepsilon\text{N} &= \gamma \times \varepsilon(\delta^{15}\text{N}-\text{NO}_3^-)_{\text{OH}} + (1 - \gamma) \times \varepsilon(\delta^{15}\text{N}-\text{NO}_3^-)_{\text{H}_2\text{O}} \\ &= \gamma \times \varepsilon(\delta^{15}\text{N}-\text{HNO}_3)_{\text{OH}} + (1 - \gamma) \times \varepsilon(\delta^{15}\text{N}-\text{HNO}_3)_{\text{H}_2\text{O}} \end{aligned} \quad (14)$$

$$\varepsilon(\delta^{15}\text{N}-\text{HNO}_3)_{\text{OH}} = \varepsilon(\delta^{15}\text{N}-\text{NO}_2)_{\text{OH}} = 1000 \times \left[\frac{(\alpha_{\text{NO}_2/\text{NO}} - 1)(1 - f_{\text{NO}_2})}{(1 - f_{\text{NO}_2}) + (\alpha_{\text{NO}_2/\text{NO}} \times f_{\text{NO}_2})} \right] \quad (15)$$

$$\varepsilon(\delta^{15}\text{N}-\text{HNO}_3)_{\text{H}_2\text{O}} = \varepsilon(\delta^{15}\text{N}-\text{N}_2\text{O}_5)_{\text{H}_2\text{O}} = 1000 \times (\alpha_{\text{N}_2\text{O}_5/\text{NO}_2} - 1) \quad (16)$$

Where, γ is the contribution of $\cdot\text{OH}$ formation pathway to NO_3^- , εN is the nitrogen isotope fractionation value. f_{NO_2} is the fraction of NO_2 in the total NO_x . $^{18}\alpha_{\text{NO}_2/\text{NO}}$, $^{18}\alpha_{\text{OH}/\text{H}_2\text{O}}$, $^{18}\alpha_{\text{N}_2\text{O}_5/\text{NO}_2}$ are the oxygen isotope equilibrium fractionation factors between NO_2 and NO , $\cdot\text{OH}$ and H_2O , N_2O_5 and NO_2 , respectively. $^{15}\alpha_{\text{NO}_2/\text{NO}}$ and $^{15}\alpha_{\text{N}_2\text{O}_5/\text{NO}_2}$ are the nitrogen isotope equilibrium fractionation factor between NO_2 and NO , N_2O_5 and NO_2 , respectively.

Table 1. The estimation of $\delta^{15}\text{N}-\text{NH}_3$ and $\delta^{15}\text{N}-\text{NO}_x$ from various sources.

Source	$\delta^{15}\text{N}-\text{NH}_3(\text{‰})$	References
Biomass burning	17.5±7.8	(Kawashima and Kurahashi, 2011; Xiao et al., 2020)
Coal combustion	-2.5±6.4	(Felix et al., 2013; Pan et al., 2016)
Urban traffic	6.6±2.1	(Walters et al., 2020)
Fertilizer	-28.3±5.8	(Bhattarai et al., 2021; Chang et al., 2016; Felix et al., 2013; Bhattarai et al., 2020)
Livestock	-18.3±7.7	(Bhattarai et al., 2021; Chang et al., 2016; Felix et al., 2013; Bhattarai et al., 2020)
Urban waste	-22.8±3.6	(Bhattarai et al., 2021; Chang et al., 2016)
Source	$\delta^{15}\text{N}-\text{NO}_x(\text{‰})$	References
Biomass burning	1.04±4.13	(Zong et al., 2017; Fibiger and Hastings, 2016; Zong et al., 2022)
Coal combustion	13.72±4.57	(Zong et al., 2017; Felix et al., 2015; Felix et al., 2012)
Mobile source	-7.25±7.80	(Zong et al., 2017; Walters et al., 2015)
Soil microbial process	-33.77±12.16	(Zong et al., 2017; Felix and Elliott, 2013)

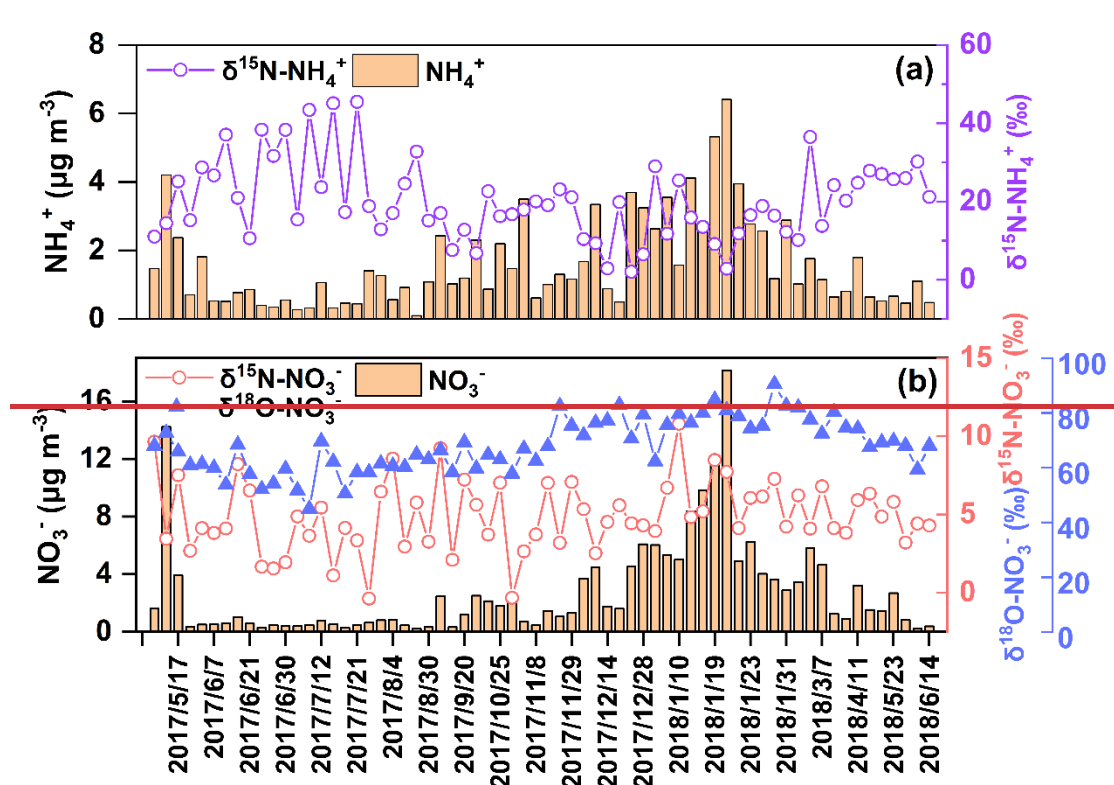
213

214 3. Results and discussion

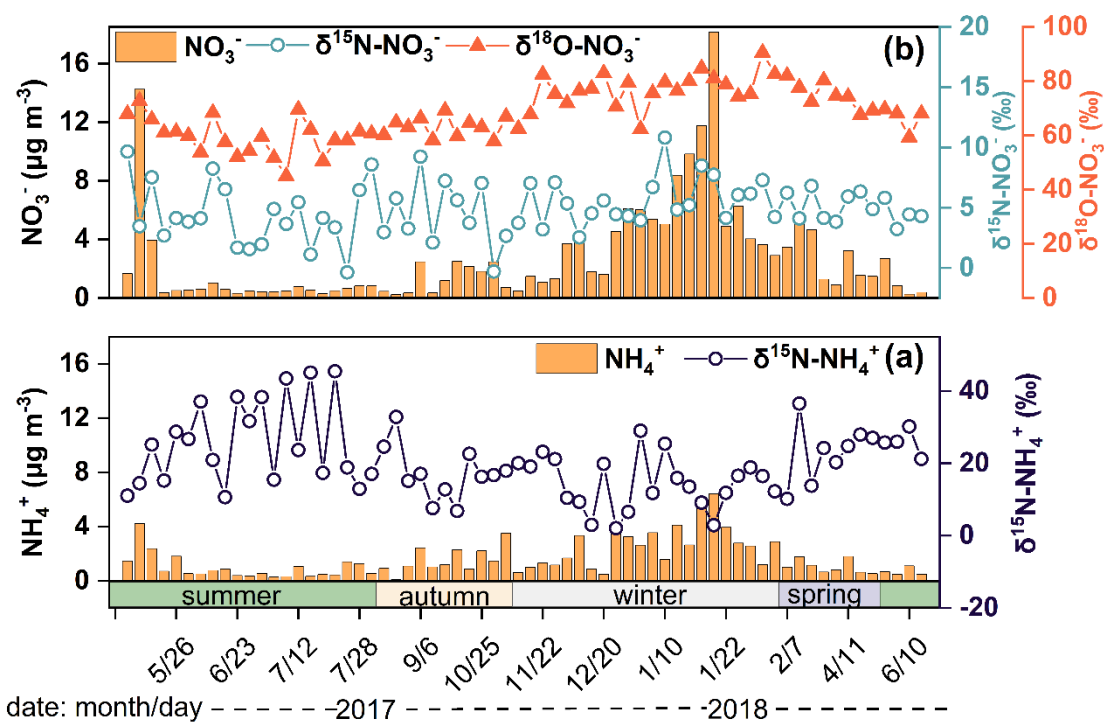
215 3.1. Concentration and seasonal variation of NH_4^+ and NO_3^-

216 The concentration of NH_4^+ and NO_3^- in $\text{PM}_{2.5}$ was $1.6 \pm 1.3 \mu\text{g m}^{-3}$ and $2.8 \pm 3.4 \mu\text{g m}^{-3}$,
 217 contributed 18.7% and 32.6% to SIA. The concentration of $\text{N}-\text{NH}_4^+$ and $\text{N}-\text{NO}_3^-$ was 1.2 ± 1.0

218 $\mu\text{g m}^{-3}$ and $0.6\pm 0.8 \mu\text{g m}^{-3}$, contributed 45.8% and 23.2% to TN, respectively; thus, NH_4^+ and
 219 NO_3^- were essential part of nitrogen aerosols. NH_4^+ and NO_3^- showed similar seasonal
 220 variations with higher concentrations in winter than in summer (**Fig. 1**). During winter the air
 221 mass was often dry and cold with low wind speed, which meant the decrease of the atmospheric
 222 self-purification capability. In addition, primary combustion sources related to fossil fuel and
 223 biomass burning always showed significant increase in North China in winter, which greatly
 224 increased the concentration of atmospheric pollutants in Guangzhou by long-range
 225 transportation. However, during summer, the air mass from sea was relatively clean with high
 226 wind speed facilitating the diffusion of pollutants. Moreover, high temperature in summer was
 227 conducive to the decomposition of NH_4NO_3 (Song et al., 2008). Thus, the levels of NH_4^+ and
 228 NO_3^- were lower in summer. In addition, concentrations of NH_4^+ and NO_3^- in our study, were
 229 lower than North China [Beijing(Wu et al., 2019; Fan et al., 2022), Tianjin(Xiang et al., 2022),
 230 Shijiazhuang(Xiang et al., 2022), and Harbin(Sun et al., 2021)], East China [Nanchang(Xiao
 231 et al., 2020)], and Central China [Wuhan and Changsha(Xiao et al., 2020; Zong et al., 2020)],
 232 suggested the level of air pollution in Guangzhou has been alleviated to a certain extent.
 233 Therefore, it is necessary to conduct comprehensive study on the emission sources of NH_4^+ and
 234 NO_3^- to take more effective measures to mitigate air pollution.



235



236

237 **Figure 1.** The concentration and $\delta^{15}\text{N}$ of NH_4^+ (a) and concentration, $\delta^{15}\text{N}$, and $\delta^{18}\text{O}$ of NO_3^-
 238 (b).

239 **3.2. Characteristic and seasonal variation in $\delta^{15}\text{N-NH}_4^+$ and source apportionment of**
 240 **NH_4^+**

241 The $\delta^{15}\text{N-NH}_4^+$ values over Guangzhou ranged from 2.1‰ to 45.5‰, with an annual mean
 242 of 20.2 ± 10.1 ‰. In our study, the $\delta^{15}\text{N-NH}_4^+$ values were comparable to those at suburban sites
 243 (Fig. S12) such as sites in Japan (22.1 ± 8.3 ‰, 16.1 ± 6.6 ‰)(Kawashima and Kurahashi, 2011)
 244 and Korea (Jeju Island, 17.4 ± 4.9 ‰)(Kundu et al., 2010) but heavier than those in polluted
 245 regions, such as Heshan in Pearl River Delta (PRD)-Guangzhou during summer haze(average \pm
 246 7.17 ‰)(Liu et al., 2018) and Beijing (-37.1 ‰ to ± 5.8 ‰)(Pan et al., 2016). $\delta^{15}\text{N-NH}_4^+$ values
 247 were lower in autumn (17.3‰) and winter (14.4‰) than in spring (22.5‰) and summer
 248 (25.7‰), which was similar to the trends in Japan(Kawashima and Kurahashi, 2011).

249 The seasonal differences in $\delta^{15}\text{N-NH}_4^+$ values were significant between warm
 250 (summer/spring) and ~~cool~~ cold seasons (winter/fall autumn) ($p < 0.05$). The $\delta^{15}\text{N-NH}_4^+$ was
 251 affected by the ratio of $\text{NH}_4^+/(\text{NH}_3+\text{NH}_4^+)$ (Text S3 Eq. (8) and Fig. S1). A linear fitting
 252 equation was observed between $\text{NH}_4^+/(\text{NH}_3+\text{NH}_4^+)$ and $\delta^{15}\text{N-NH}_4^+$, and the absolute value of

253 the slope (32.4) approximated the isotope equilibrium fractionation value ($+33\%$) between
254 atmospheric NH_3 and NH_4^+ (Fig. S21). The linear fitting suggested that the lower the NH_4^+
255 proportion was, the heavier the $\delta^{15}\text{N-NH}_4^+$ value. The lower NH_4^+ level was accordance with
256 higher $\delta^{15}\text{N-NH}_4^+$ in summer, which was the opposite of winter. In addition, previous study
257 suggested that the marked variation in $\delta^{15}\text{N-NH}_4^+$ values was largely controlled by the emission
258 sources of NH_3 , the precursor gas of NH_4^+ (Liu et al., 2018). According to the $\delta^{15}\text{N-NH}_4^+$ results,
259 the source of NH_4^+ was assigned as biomass burning ($27.9\pm 16.4\%$), coal combustion
260 ($16.0\pm 3.9\%$), vehicles ($19.8\pm 5.3\%$), fertilizer ($10.9\pm 6.1\%$), livestock ($12.7\pm 5.8\%$), and urban
261 waste ($11.9\pm 6.1\%$), shown in Fig. 2a.

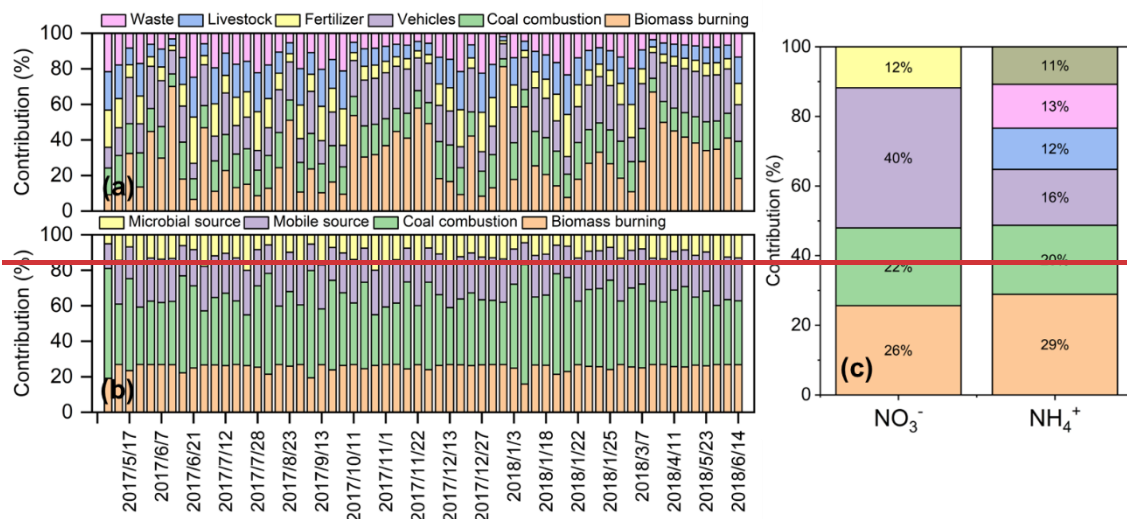
262 In our study, non-agriculture sources were the dominators of NH_4^+ ($75.6\pm 1\%$).
263 Unexpectedly, the contribution of biomass burning was the highest. Especially, from late June
264 to July, the contribution of biomass burning enhanced, which possibly resulted from sugarcane
265 leaf burning. The $\delta^{15}\text{N}$ in sugarcane leaf was as high as 38% (Martinellia et al., 2002). ~~The~~
266 ~~$\delta^{15}\text{N-NH}_4^+$ released from sugarcane leaf was estimated as 44.1% (SI Text S4), which coincided~~
267 ~~with the highest $\delta^{15}\text{N-NH}_4^+$ value in July (45.5% and 45.1%). The $\delta^{15}\text{N}$ of NH_4^+ formed from~~
268 ~~NH_3 released by sugarcane leaves burning was 44.1% (SI Text S3), which was consistent with~~
269 ~~the highest $\delta^{15}\text{N-NH}_4^+$ values (45.5% and 45.1%) in July.~~ In PRD, south winds prevail in July
270 and the sampling site is located downwind of sugarcane planting area. Therefore, the air mass
271 to the sampling site might carry the pollutants related to sugarcane leaf burning. K^+ is a typical
272 biomass burning tracer (Cui et al., 2018). Considering the impact of primary emission intensity,
273 $[\text{NH}_4^+/\text{EC}]$ and $[\text{K}^+/\text{EC}]$ were used to calculate the correlation coefficient ($r=0.435$, $p < 0.01$),
274 which verified NH_4^+ was influenced by biomass burning. In recent years, biomass burning has
275 been gradually identified as an important source of NH_4^+ (Meng et al., 2017; Xiao et al., 2020).
276 The results based on emission inventories showed that the contribution of residential biomass
277 combustion to NH_3 ranged from 33% to 53% in China (Meng et al., 2017). According to $\delta^{15}\text{N}$,
278 biomass burning contributed 18% [Harbin, East North China] (Sun et al., 2021), 46% [Wuhan,
279 South Central China], 40% [Changsha, South Central China] (Xiao et al., 2020), 35%
280 [Nanchang, East China] (Xiao et al., 2020), and 23% [Guangzhou, South China] (Chen et al.,
281 2022a) to NH_4^+ . Particularly, in Guangzhou the contribution of biomass burning in the ground
282 was higher than that in Guangzhou tower with the a height of 488 meters, suggested that the

283 influence of regional biomass burning(Chen et al., 2022a). Furthermore, ⁷Be~~is~~ mainly
284 ~~originated~~originates from upper atmosphere, whereas ²¹⁰Pb is derived from terrestrial
285 surface(Jiang et al., 2021b). High level of ⁷Be observed in ground suggested the sink influence
286 of upper atmosphere. ⁷Be and ²¹⁰Pb are chemically stable and with unique sources, which can
287 effectively reflect the transport of continental air mass and the air exchange between
288 stratosphere and troposphere. In our study, the correlation coefficient between NH₄⁺ and ²¹⁰Pb
289 (r=0.701, *p* < 0.01) was higher than that between NH₄⁺ and ⁷Be (r=0.432, *p* < 0.01), suggested
290 that NH₄⁺ was mainly affected by regional emission. Therefore, biomass burning exerted
291 essential influence on NH₄⁺ level, which should no longer be ignored.

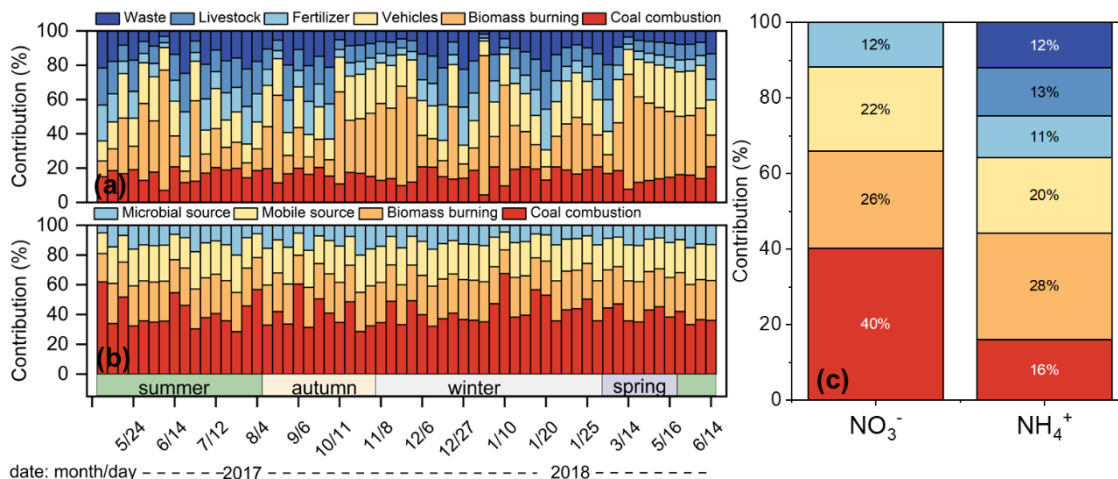
292 In addition, with the acceleration of urbanization, combustion sources related to fossil
293 fuels have become the main sources of NH₃. In previous studies, the source of NH_x (NH₃+NH₄⁺)
294 was mainly from ~~agriculture~~agricultural activity due to rough way of farming(Chang et al.,
295 2016; Pan et al., 2020). However, with the improvement of efficient fertilization practices,
296 agricultural NH₃ decreased significantly(Wang et al., 2022). Fossil fuels, such as coal and
297 gasoline, are major energies for production and domestic using, and their contribution to NH₃
298 has become increasingly important. In North China, fossil fuel combustion contributed 92% to
299 NH₃ during hazes(Zhang et al., 2020; Pan et al., 2016). In previous study of Guangzhou, the
300 contribution of NH₃ from fossil source in ground observations (43%) was higher than the
301 observed in Guangzhou tower (18%), indicated the importance of locally related fossil fuel
302 combustion source(Chen et al., 2022a). In our study, vehicle emission and coal combustion
303 contributed 19.8±5.3% and 16.0±3.9% of NH₄⁺ respectively, which was lower than ~~the~~North
304 China but higher than agricultural sources. The share of NH₃ from vehicle exhaust was
305 estimated to be 18.8% based on the emission factor of NH₃ from on road vehicles in Guangzhou,
306 which was similar to our results(Liu et al., 2014). The selective catalytic reduction process for
307 vehicle can reduce NO_x, but increased emission of NH₃, which has confirmed as an important
308 source of NH₃(Heeb et al., 2006; Meng et al., 2017). Despite the efforts of government to
309 promote electric vehicles in recent years, their share is still relatively low (about 5%). As
310 increasing car ownership, this has an important impact on atmospheric NH₃. Coal combustion
311 was the second most important source of fossil combustion after vehicle emissions in our study,
312 although the contribution was lower than in North China(Wu et al., 2019; Zhang et al., 2020;

313 Pan et al., 2016). The absence of heating in Guangzhou may explain the lower contribution of
 314 coal combustion compared to the North. On an annual basis, the contribution of fossil fuel-
 315 related combustion sources in our study (35.8%) was comparable to that in North China (37%-
 316 52%)(Pan et al., 2018a).

317 The source contributions of NH_4^+ in our study were compared to other regions, shown in
 318 **Fig. S3**. The combustion related sources (biomass burning, coal combustion, and vehicle) have
 319 gradually become the dominant source of urban atmospheric NH_3 . Biomass burning and
 320 vehicle could emit massive carbon monoxide (CO)(Li and Wang, 2007; Wang et al., 2005). In
 321 Guangzhou, NH_4^+ was positively related to CO ($r=0.637$, $p < 0.01$), which confirmed
 322 combustion sources ~~playing~~ played a key role in NH_4^+ . From a historical perspective, NH_3
 323 emissions from anthropogenic combustion and industry have been steadily increasing since
 324 1960(Meng et al., 2017). The optimization of energy structure and encouragement of the
 325 development of new energy vehicle would be hopeful to reduce NH_3 . The results of this study
 326 would be conducive to ~~reduce~~ reducing NH_3 scientifically and effectively, and would relieve
 327 the pressure on the reduction from agricultural source.



328



329

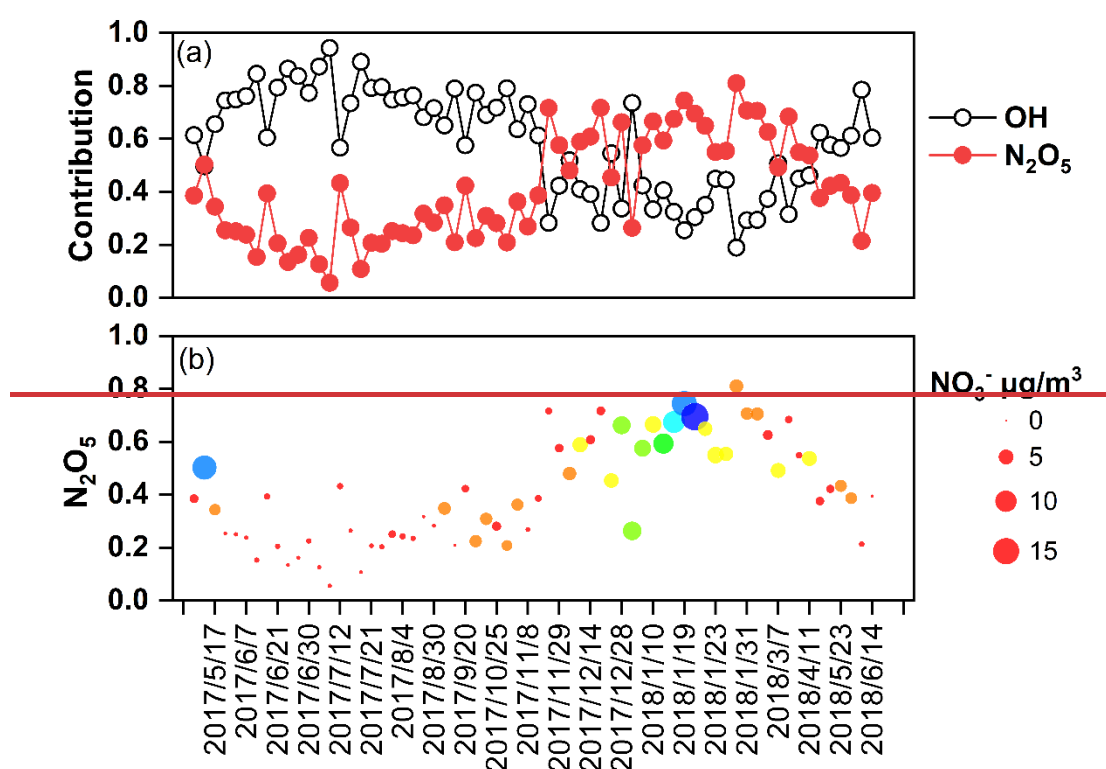
330 **Figure 2.** The sources apportionment results of atmospheric NH₄⁺ (a) and NO₃⁻ (b) in
 331 Guangzhou, and the comparison of sources results between NH₄⁺ and NO₃⁻ (c).

332 **3.3. Characteristic and seasonal variation in $\delta^{18}\text{O}-\text{NO}_3^-$ and $\delta^{15}\text{N}-\text{NO}_3^-$ and source**
 333 **apportionment of NO₃⁻**

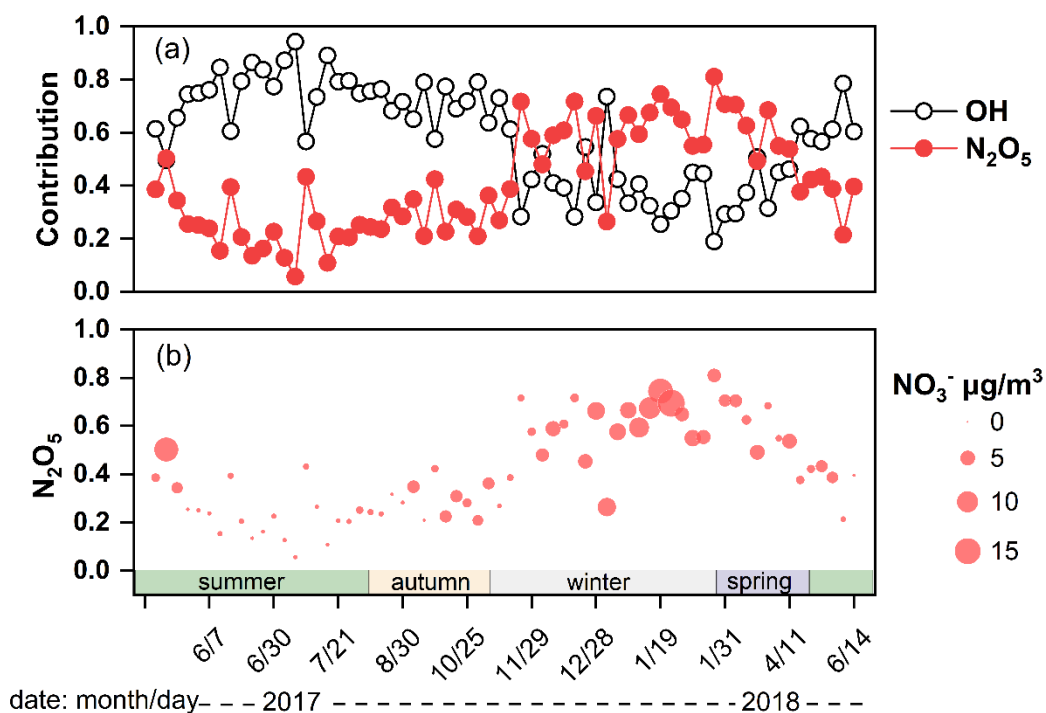
334 **3.3.1. Seasonal variation of $\delta^{18}\text{O}-\text{NO}_3^-$**

335 The $\delta^{18}\text{O}-\text{NO}_3^-$ in Guangzhou was $68.1 \pm 9.7\text{‰}$ (44.9‰ to 90.5‰) comparable to that in
 336 precipitation ($66.3 \pm 2.8\text{‰}$, ranging from 33.4‰ to 86.2‰)(Fang et al., 2011), but lower than
 337 those regions with weak light intensity, such as BeiChengHuanghuangcheng Island
 338 ($76.6 \pm 8.1\text{‰}$, ranging from 49.4‰ to 103.9‰)(Zong et al., 2017) and Bermuda Islands
 339 ($71.1 \pm 3.0\text{‰}$, cold season $76.9 \pm 6.3\text{‰}$) (Hastings et al., 2003). In this study, $\delta^{18}\text{O}-\text{NO}_3^-$ was
 340 higher in winter and spring than in summer and autumn, which was similar to the seasonal
 341 variation in $\delta^{18}\text{O}-\text{NO}_3^-$ in previous studies (Fang et al., 2011; Gobel et al., 2013). On the one
 342 hand, $\delta^{18}\text{O}-\text{NO}_3^-$ value was associated with the formation pathways of NO₃⁻. The results
 343 simulated by Bayesian mixing model suggested that the contributions of N₂O₅ channel to NO₃⁻
 344 were 56.8%, 58.9%, 29.2%, and 27.0% in winter, spring, ~~fall~~autumn, and summer, respectively.
 345 The $\delta^{18}\text{O}$ value of NO₃⁻ formed by N₂O₅ channel is higher than that by ·OH pathway (SI Text
 346 S52). The night in cold season was longer than that in warm season, which favored NO₃⁻
 347 formation through N₂O₅ channel. In addition, the illumination intensity was weakened in cold
 348 season compared with that in warm season, which constrained the production of ·OH(Zong et
 349 al., 2020; Tan et al., 2019; Wang et al., 2017). Thus, the contribution of the N₂O₅ channel in

350 cold season was higher than that in warm season. Furthermore, concentration of NO_3^- was high
 351 when contribution of N_2O_5 channel enhanced (Fig. 3), suggested NO_3^- pollution was related to
 352 N_2O_5 hydrolysis pathway. The air mass to Guangzhou was derived from the South China Sea
 353 in summer and the North continental region in winter. The higher $\delta^{18}\text{O}-\text{NO}_3^-$ and NO_3^-
 354 concentration might be affected by long-range and high-altitude transport from North China,
 355 which might carry abundant NO_x precursors. Massive NO_3^- could be formed by N_2O_5 hydrolysis
 356 at high altitude and transported to the ground. The index of $f(^7\text{Be}, ^{210}\text{Pb})$ was expressed in SI
 357 Text S1 and could reflect the influence of atmospheric dynamic transport on aerosol
 358 pollutants (Jiang et al., 2021b). Generally, air masses with low values of $f(^7\text{Be}, ^{210}\text{Pb})$ suggested
 359 that pollutants were associated with continental surface emission, whereas high $f(^7\text{Be}, ^{210}\text{Pb})$
 360 were influenced by long-range transport from upper air masses. The contribution of N_2O_5
 361 channel was positively correlated with $f(^7\text{Be}, ^{210}\text{Pb})$ ($r=0.319$, $p < 0.05$), indicated the long-
 362 range transport influence of upper air mass on N_2O_5 channel. For example, on 25 January 2018,
 363 the contribution of N_2O_5 channel (nitrate) was 81.1% ($3.6 \mu\text{g m}^{-3}$), when the upper air mass
 364 was from the North China. However, on 7 July 2017, the N_2O_5 channel (nitrate) contributed
 365 only 5.7% ($0.5 \mu\text{g m}^{-3}$) corresponding to the air mass mainly from the South China Sea
 366 transported at low-altitude (Fig. S4).



367



368

369 **Figure 3.** The contribution of the OH radical oxidation and N₂O₅ hydrolysis pathway to NO₃⁻
 370 (a). The vertical position of dots corresponded to the contribution of N₂O₅ pathway and the size
 371 of the dots corresponded to the concentration of NO₃⁻ (b).

372 $\delta^{18}\text{O}-\text{NO}_3^-$ decreased from 76.7‰ in 2014 to 68.1‰ in 2017-2018 (Zong et al., 2020),
 373 which indicated that $\cdot\text{OH}$ channel became more important in Guangzhou. The enhanced
 374 contribution of $\cdot\text{OH}$ pathway indicated the increasing atmospheric oxidation capacity. In recent
 375 years, although the concentration of PM_{2.5} in Guangzhou has significantly decreased, the
 376 photochemical pollution caused by high O₃ concentrations was not optimistic (Tan et al., 2019).
 377 The O₃ concentration in the PRD showed a fluctuating upward trend from 2013 to 2020;
 378 especially in 2017-2018, O₃ concentrations were at high levels (Environmental Status Bulletin
 379 of Guangdong Province Fig. S5). In our study, the NO₃⁻ formation pathway inferred from $\delta^{18}\text{O}-$
 380 NO₃⁻ proved the enhancement of atmospheric oxidation capacity.

381 3.3.2. Seasonal variation of $\delta^{15}\text{N}-\text{NO}_3^-$ and source apportionment of NO₃⁻

382 **Seasonal variation of $\delta^{15}\text{N}-\text{NO}_3^-$.** The $\delta^{15}\text{N}-\text{NO}_3^-$ in Guangzhou was $4.9 \pm 2.2\text{‰}$ (-0.4‰
 383 to 10.8‰), which was similar to the wet deposition (Fang et al., 2011). The $\delta^{15}\text{N}-\text{NO}_3^-$ was
 384 comparable to that from the Northeast United States (6.8‰) (Elliott et al., 2009), and lower

385 than regions in China, where NO_3^- was predominantly derived from anthropogenic sources,
386 such as Heshan in Guangdong ($7.50 \pm 3.30\%$)(Su et al., 2020), BeiChengHuanghuangcheng
387 Island ($8.20 \pm 6.20\%$)(Zong et al., 2017), and Beijing ($12.1 \pm 3.3\%$)(Fan et al., 2022).
388 Nevertheless, the $\delta^{15}\text{N}-\text{NO}_3^-$ in this study was significantly higher than those from clean
389 background regions, where NO_3^- was mainly from natural sources, such as the coast of
390 Antarctica (-12.4 ± 7.20 - $12.0 \pm 15.6\%$)(Savarino et al., 2007) and Bermuda ($-2.1 \pm 1.5\%$ warm
391 season, $-5.9 \pm 3.3\%$ ~~cool~~ cold season)(Hastings et al., 2003). The values of $\delta^{15}\text{N}-\text{NO}_3^-$ in winter,
392 spring, summer, and autumn were 5.6‰, 5.3‰, 4.4‰, and 4.5‰, respectively. The $\delta^{15}\text{N}-\text{NO}_3^-$
393 in winter and summer showed significant difference ($p < 0.05$). The values of $\delta^{15}\text{N}-\text{NO}_3^-$ were
394 influenced by atmospheric processes and emission sources(Elliott et al., 2009). For N_2O_5
395 channel, NO_3^- is characterized by higher $\delta^{15}\text{N}$ values(Freyer et al., 1993; Elliott et al., 2009).
396 The N_2O_5 channel was the predominant formation pathway of NO_3^- in winter, which was in
397 accordance with the seasonal variation in $\delta^{15}\text{N}-\text{NO}_3^-$. In addition, the difference in $\delta^{15}\text{N}-\text{NO}_3^-$
398 reflected the variation in the emission source of NO_3^- . $\delta^{15}\text{N}-\text{NO}_x$ from coal combustion was
399 relatively high. In winter, the higher $\delta^{15}\text{N}-\text{NO}_3^-$ was probably related to long-range transport
400 from North, where coal combustion enhanced in winter.

401 **Source apportionment of NO_3^- .** Based on the Bayesian mixing model coupled with $\delta^{15}\text{N}-$
402 NO_3^- , NO_3^- sources were assigned as coal combustion $40.4 \pm 8.7\%$, biomass burning $25.6 \pm 2.1\%$,
403 mobile sources (vehicles) $22.3 \pm 3.1\%$, and microbial process $11.7 \pm 3.8\%$. **Figure 2b** and **Figure**
404 **Fig. S6** showed the source contribution of NO_3^- in Guangzhou and other regions in China,
405 respectively. Compared to earlier periods (2013-2014), the concentration of NO_3^- from vehicle
406 and coal combustion decreased significantly(Zong et al., 2020), which resulted from the stricter
407 vehicle emission standard, promotion of new energy electric vehicles, and ultraclean
408 transformation of coal combustion(Guangdongprovince, 2014; Tang et al., 2019). However,
409 almost all production and domestic segments rely on energy generated from coal combustion,
410 which was still dominant source of NO_3^- in 2017-2018. Coal combustion was affected not only
411 by local emissions but also by external air mass transmission. The contribution of coal
412 combustion was higher in winter than in summer, which probably related to the long-range
413 transportation from the North. Taking 10 January 2018 as an example, the contribution of coal
414 combustion sources to NO_3^- was 67.5%, and the corresponding air mass was from the North

415 and transmitted to Guangzhou through high altitude. However, the air mass on 26 July 2017
416 ~~were was~~ mainly from the South China Sea, which was transmitted through low-altitude to
417 Guangzhou. The contribution of coal burning to NO_3^- on 26 July 2017 was 28.5% lower than
418 that on 10 January 2018.

419 As non-fossil combustion source, biomass burning was also an important source of NO_3^-
420 and accounted for 25.6%. The contribution of biomass burning and vehicle was stable
421 throughout a year. Generally, high intensity biomass burning occurred in winter in Guangdong
422 province (dry season, i.e., from November to March)(Xu et al., 2019). K^+ is a typical tracer of
423 biomass burning. The concentration of K^+ enhanced in winter ($0.4\mu\text{g}/\text{m}^3$) was higher than that
424 in summer ($0.2\mu\text{g}/\text{m}^3$) and autumn ($0.2\mu\text{g}/\text{m}^3$), respectively, indicating enhancement of
425 biomass burning intensity. Also, NO_3^- concentration of biomass burning remarkably enhanced
426 in winter ($1.2\mu\text{g}/\text{m}^3$), and was higher than that in summer ($0.4\mu\text{g}/\text{m}^3$) and autumn ($0.3\mu\text{g}/\text{m}^3$),
427 respectively. However, coal combustion also enhanced in winter due to the demand for heating
428 in North China. Our sampling site was influenced by the air mass with high coal combustion
429 contribution from the North by long-range transportation, which may reduce the contribution
430 of biomass burning relatively. Thus, the contribution of biomass burning showed stable
431 compared with coal combustion. Another non-fossil source is related to soil microbial activity
432 and only contributed 11.7% to NO_3^- , which was unexpectedly lower than the results in earlier
433 periods (2013-2014). Generally, the microorganisms in soil emit NO through nitrification or
434 denitrification, which was affected by the amount of carbon and nitrogen nutrients in soil(Hall
435 and Matson, 1996). In earlier periods, due to the higher level of aerosols, the amount of
436 nutrients settling in soil was also higher, which was exemplified by the observation of dry and
437 wet deposition in Guangzhou(He et al., 2022; Zheng et al., 2020). In addition, the reduction of
438 cultivated land from 2013 to 2018 might also reduce the contribution of microbial source
439 emissions. Therefore, emissions from natural sources were also influenced by human activities
440 to some extent. The contribution of microbial process was higher in summer than in winter. In
441 summer, higher RH and temperature were favorable for the intense activity of soil
442 microorganisms(Zong et al., 2017). The contributions of microbial processes to NO_3^- also
443 decreased in winter compared with summer at regional background sites and five Chinese
444 megacities, including Guangzhou(Zong et al., 2017; Zong et al., 2020).

445 The sources comparison between NO_3^- and NH_4^+ was shown in Fig. 2c. Coal combustion,
446 biomass burning, and vehicles were three significant sources of NO_3^- and NH_4^+ . Coal
447 combustion and biomass burning were the dominant sources of NO_3^- and NH_4^+ , respectively.
448 The vehicles were also an important source of atmospheric inorganic N_r contributed to 22.3%
449 and 19.8% ~~to~~ of NO_3^- and NH_4^+ , respectively. Recently, the government has actively taken
450 many measures to reduce the pollution from vehicles, such as stricter automobile emission
451 standards and the promotion of new energy vehicles. However, due to the large vehicle
452 ownership base, the pollutants emitted from vehicles are not optimistic. In addition, vehicles
453 emissions could contribute half of the fresh secondary organic aerosol in urban
454 environment(Zhang et al., 2022; Zhao et al., 2022a).

455 4. Conclusions

456 A year-long field observation was conducted in Guangzhou to clarify the atmospheric fate
457 of inorganic nitrogen aerosol. Inorganic nitrogen species were the most essential component of
458 TN including NH_4^+ (45.8%) and NO_3^- (23.2%), which are also dominant components of SIA
459 and play a key role in China haze. The $\delta^{15}\text{N}$ is a powerful tool to quantify the source
460 contribution of NH_4^+ and NO_3^- , which suggested that anthropogenic combustion sources (coal
461 combustion, biomass burning, and vehicles) were the dominant sources.

462 Anthropogenic combustion sources contributed 63.2% to NH_4^+ higher than agricultural
463 sources (23.6%). NH_3 largely facilitates the formation of sulfate and nitrate. Meanwhile, sulfate
464 and nitrate promote each other with positive feedback effect, which could trigger haze. In
465 megacities of China, the focus of NH_3 reduction should be on anthropogenic combustion
466 sources, especially on biomass burning, which might be responsible for the lag of the decline
467 in the deposition of air pollutions behind the reduction in emission(Zhao et al., 2022b). In
468 addition, anthropogenic combustion sources accounted for 88.3% of NO_3^- . Coal combustion
469 and vehicles contributed 40.4% and 22.3% to NO_3^- , respectively. Despite a series of measures
470 to reduce emissions of NO_x , fossil fuels, as the main energy for production and living, will still
471 inevitably emit a large amount of NO_x . Our results emphasized that the emission of
472 atmospheric inorganic nitrogen is largely related to anthropogenic combustion sources. The

473 development and promotion of clean energy and efficient use of biomass are conducive to the
474 deep reduction of atmospheric nitrogen.

475 **Data availability**

476 The original data of this research (stable nitrogen isotopes and inorganic nitrogen
477 concentrations) are available at Mendeley data (Li and Li, 2023). The Iso Source model was
478 downloaded from Environmental Protection Agency, via their website:
479 https://www.epa.gov/sites/default/files/2015-11/isosourcev1_3_1.zip.

480 **Author contributions**

481 Funding acquisition: Jun Li

482 Investigation: Tingting Li, Zeyu Sun, and Hongxing Jiang

483 Methodology: Tingting Li, Zeyu Sun, Hongxing Jiang, Jun Li, and Chongguo Tian

484 Project Administration: Jun Li

485 Resources: Jun Li, Chongguo Tian, and Gan Zhang

486 Software: Tingting Li, [Zeyu Sun, and Chongguo Tian](#)

487 Validation: Tingting Li and Jun Li

488 Writing – original draft: Tingting Li

489 Writing – review & editing: Jun Li

490 **Competing interests**

491 The authors declare that they have no conflict of interest.

492 **Financial support**

493 This study was supported by the Natural Science Foundation of China (NSFC; Nos.
494 (41977177), Guangdong Basic and Applied Basic Research Foundation (2021A1515011456),
495 Guangdong Foundation for Program of Science and Technology Research (Grant No.
496 2019B121205006 and 2020B1212060053).

497 **References**

- 498 Baskaran, M., K., B. S., and F., M. D.: Oxygen isotope dynamics of atmospheric nitrate and its precursor molecules.
499 In Handbook of Environmental Isotope Geochemistry., Springer-Verlag Berlin Heidelberg 2011.
- 500 Bhattarai, H., Zhang, Y. L., Pavuluri, C. M., Wan, X., Wu, G., Li, P., Cao, F., Zhang, W., Wang, Y., Kang, S., Ram,
501 K., Kawamura, K., Ji, Z., Widory, D., and Cong, Z.: Nitrogen speciation and isotopic composition of aerosols
502 collected at Himalayan Forest (3326 m a.s.l.): seasonality, sources, and implications, Environ. Sci. Technol.,
503 53, 12247-12256, <https://doi.org/10.1021/acs.est.9b03999>, 2019.
- 504 Bhattarai, N., Wang, S., Pan, Y., Xu, Q., Zhang, Y., Chang, Y., and Fang, Y.: $\delta^{15}\text{N}$ -stable isotope analysis of NH_3 :
505 An overview on analytical measurements, source sampling and its source apportionment, Front. Environ. Sci.
506 Eng., 15, 126, <https://doi.org/10.1007/s11783-021-1414-6>, 2021.
- 507 Bhattarai, N., Wang, S., Xu, Q., Dong, Z., Chang, X., Jiang, Y., and Zheng, H.: Sources of gaseous NH_3 in urban
508 Beijing from parallel sampling of NH_3 and NH_4^+ , their nitrogen isotope measurement and modeling, Sci.
509 Total Environ., 747, 141361, <https://doi.org/10.1016/j.scitotenv.2020.141361>, 2020.
- 510 Breemen, N. V.: Nitrogen cycle natural organic tendency, Nature, 415, <https://doi.org/10.1038/415381a>, 2002.
- 511 Chang, Y., Liu, X., Deng, C., Dore, A. J., and Zhuang, G.: Source apportionment of atmospheric ammonia before,
512 during, and after the 2014 APEC summit in Beijing using stable nitrogen isotope signatures, Atmos. Chem.
513 Phys., 16, 11635-11647, <https://doi.org/10.5194/acp-16-11635-2016>, 2016.
- 514 Chen, Z., Pei, C., Liu, J., Zhang, X., Ding, P., Dang, L., Zong, Z., Jiang, F., Wu, L., Sun, X., Zhou, S., Zhang, Y.,
515 Zhang, Z., Zheng, J., Tian, C., Li, J., and Zhang, G.: Non-agricultural source dominates the ammonium
516 aerosol in the largest city of South China based on the vertical $\delta^{15}\text{N}$ measurements, Sci. Total Environ., 848,
517 157750, <https://doi.org/10.1016/j.scitotenv.2022.157750>, 2022a.
- 518 Chen, Z. L., Song, W., Hu, C. C., Liu, X. J., Chen, G. Y., Walters, W. W., Michalski, G., Liu, C. Q., Fowler, D.,
519 and Liu, X. Y.: Significant contributions of combustion-related sources to ammonia emissions, Nat.
520 Commun., 13, 7710, <https://doi.org/10.1038/s41467-022-35381-4>, 2022b.
- 521 Cui, M., Chen, Y., Zheng, M., Li, J., Tang, J., Han, Y., Song, D., Yan, C., Zhang, F., Tian, C., and Zhang, G.:
522 Emissions and characteristics of particulate matter from rainforest burning in the Southeast Asia, Atmos.
523 Environ., 191, 194-204, <https://doi.org/10.1016/j.atmosenv.2018.07.062>, 2018.
- 524 Dunne, E. M., Gordon, H., Kürten, A., Almeida, J., Duplissy, J., Williamson, C., Ortega, I. K., Pringle, K. J.,
525 Adamov, A., and Schobesberger, S.: Global atmospheric particle formation from cern cloud measurements,
526 Science, 354, 1119-1123, <https://doi.org/10.1126/science.aaf2649>, 2016.
- 527 Elliott, E. M., Kendall, C., Wankel, S. D., Burns, D. A., Boyer, E. W., Harlin, K., Bain, D. J., and Butler, T. J.:
528 Nitrogen isotopes as indicators of NO_x source contributions to atmospheric nitrate deposition across the
529 midwestern and Northeastern United States, Environ. Sci. Technol., 41, 7661-7667,
530 <https://doi.org/10.1021/es070898t>, 2007.
- 531 Elliott, E. M., Kendall, C., Boyer, E. W., Burns, D. A., Lear, G. G., Golden, H. E., Harlin, K., Bytnerowicz, A.,
532 Butler, T. J., and Glatz, R.: Dual nitrate isotopes in dry deposition: Utility for partitioning NO_x source
533 contributions to landscape nitrogen deposition, J. Geophys. Res. , 114,
534 <https://doi.org/10.1029/2008JG000889>, 2009.
- 535 Fan, M.-Y., Zhang, Y.-L., Hong, Y., Lin, Y.-C., Zhao, Z.-Y., Cao, F., Sun, Y., Guo, H., and Fu, P.: Vertical
536 differences of nitrate sources in urban boundary layer based on tower measurements, Environ. Sci. Technol.
537 Lett., 2c00600, <https://doi.org/10.1021/acs.estlett.2c00600>, 2022.
- 538 Fan, M. Y., Zhang, Y. L., Lin, Y. C., Cao, F., Zhao, Z. Y., Sun, Y., Qiu, Y., Fu, P., and Wang, Y.: Changes of emission
539 sources to nitrate aerosols in Beijing after the clean air actions: evidence from dual isotope compositions, J.
540 Geophys. Res.: Atmos., 125, 031998, <https://doi.org/10.1029/2019jd031998>, 2020.

541 Fang, Y. T., Koba, K., Wang, X. M., Wen, D. Z., Li, J., Takebayashi, Y., Liu, X. Y., and Yoh, M.: Anthropogenic
542 imprints on nitrogen and oxygen isotopic composition of precipitation nitrate in a nitrogen-polluted city in
543 southern China, *Atmos. Chem. Phys.*, 11, 1313-1325, <https://doi.org/10.5194/acp-11-1313-2011>, 2011.

544 Felix, J. D. and Elliott, E. M.: The agricultural history of human-nitrogen interactions as recorded in ice core $\delta^{15}\text{N}$ -
545 NO_3^- , *Geophys. Res. Lett.*, 40, 1642-1646, <https://doi.org/10.1002/grl.50209>, 2013.

546 Felix, J. D., Elliott, E. M., and Shaw, S. L.: Nitrogen isotopic composition of coal-fired power plant NO_x :
547 influence of emission controls and implications for global emission inventories, *Environ. Sci. Technol.*, 46,
548 3528-3535, <https://doi.org/10.1021/es203355v>, 2012.

549 Felix, J. D., Elliott, E. M., Gish, T. J., McConnell, L. L., and Shaw, S. L.: Characterizing the isotopic composition
550 of atmospheric ammonia emission sources using passive samplers and a combined oxidation-bacterial
551 denitrifier approach, *Rapid Commun. Mass Spectrom.*, 27, 2239-2246, <https://doi.org/10.1002/rcm.6679>,
552 2013.

553 Felix, J. D., Elliott, E. M., Avery, G. B., Kieber, R. J., Mead, R. N., Willey, J. D., and Mullaugh, K. M.: Isotopic
554 composition of nitrate in sequential Hurricane Irene precipitation samples: Implications for changing NO_x
555 sources, *Atmos. Environ.*, 106, 191-195, <https://doi.org/10.1016/j.atmosenv.2015.01.075>, 2015.

556 Fibiger, D. L. and Hastings, M. G.: First Measurements of the Nitrogen Isotopic Composition of NO_x from
557 Biomass Burning, *Environ. Sci. Technol.*, 50, 11569-11574, <https://doi.org/10.1021/acs.est.6b03510>, 2016.

558 Freyer, H. D., Kley, D., Volz-Thomas, A., and Kobel, K.: On the interaction of isotopic exchange processes with
559 photochemical reactions in atmospheric oxides of nitrogen, *J. Geophys. Res.*, 98, 14,791-714,796,
560 <https://doi.org/10.1029/93JD00874>, 1993.

561 Fu, X., Wang, S., Xing, J., Zhang, X., Wang, T., and Hao, J.: Increasing ammonia concentrations reduce the
562 effectiveness of particle pollution control achieved via SO_2 and NO_x emissions reduction in East China,
563 *Environ. Sci. Technol. Lett.*, 4, 221-227, <https://doi.org/10.1021/acs.estlett.7b00143>, 2017.

564 Galloway, J. N., Dentener, F. J., Capone, D. G., Boyer, E. W., Howarth, R. W., Seitzinger, S. P., Asner, G. P.,
565 Cleveland, C. C., Green, P. A., Holland, E. A., Karl, D. M., Michaels, A. F., Porter, J. H., Townsend, A. R.,
566 and Vörösmarty, C. J.: Nitrogen cycles past present and future, *Biogeochemistry*, 70, 153-226,
567 <https://doi.org/10.1007/s10533-004-0370-0>, 2004.

568 Gobel, A. R., Altieri, K. E., Peters, A. J., Hastings, M. G., and Sigman, D. M.: Insights into anthropogenic nitrogen
569 deposition to the North Atlantic investigated using the isotopic composition of aerosol and rainwater nitrate,
570 *Geophys. Res. Lett.*, 40, 5977-5982, <https://doi.org/10.1002/2013gl058167>, 2013.

571 Action Plan for Air Pollution Control of Guangdong Province (2014-2017):
572 http://www.gd.gov.cn/gkmlpt/content/0/142/mpost_142687.html, last access: February 14, 2014.

573 Hall, S. J. and Matson, P. A.: NO_x emissions from soil: implications for air quality modeling in agricultural regions,
574 *Annu. Rev. Energy Environ.*, 21, 311-346, <https://doi.org/10.1146/annurev.energy.21.1.311>, 1996.

575 Hastings, M. G., Sigman, D. M., and Lipschultz, F.: Isotopic evidence for source changes of nitrate in rain at
576 Bermuda, *J. Geophys. Res.: Atmos.*, 108, 1-12, <https://doi.org/10.1029/2003jd003789>, 2003.

577 He, S., Huang, M., Zheng, L., Chang, M., Chen, W., Xie, Q., and Wang, X.: Seasonal variation of transport
578 pathways and potential source areas at high inorganic nitrogen wet deposition sites in southern China, *J.*
579 *Environ. Sci. (China)*, 114, 444-453, <https://doi.org/10.1016/j.jes.2021.12.024>, 2022.

580 Heaton, T. H. E., Spiro, B., and Robertson, S. M. C.: Potential canopy influences on the isotopic composition of
581 nitrogen and sulphur in atmospheric deposition, *Oecologia*, 109, 600-607, 1997.

582 Heeb, N. V., Forss, A.-M., Brühlmann, S., Lüscher, R., Saxer, C. J., and Hug, P.: Three-way catalyst-induced
583 formation of ammonia—velocity- and acceleration-dependent emission factors, *Atmos. Environ.*, 40, 5986-
584 5997, <https://doi.org/10.1016/j.atmosenv.2005.12.035>, 2006.

585 Hodas, N., Sullivan, A. P., Skog, K., Keutsch, F. N., Collett, J. L., Jr., Decesari, S., Facchini, M. C., Carlton, A.
586 G., Laaksonen, A., and Turpin, B. J.: Aerosol liquid water driven by anthropogenic nitrate: implications for
587 lifetimes of water-soluble organic gases and potential for secondary organic aerosol formation, *Environ. Sci.*
588 *Technol.*, 48, 11127-11136, <https://doi.org/10.1021/es5025096>, 2014.

589 Holland, E. A., Dentener, F. J., Braswell, B. H., and Sulzman, J. M.: Contemporary and pre-industrial global
590 reactive nitrogen budgets, *Biogeochemistry*, 46, 7-43, <https://doi.org/10.1007/BF01007572>, 1999.

591 Huang, S., Elliott, E. M., Felix, J. D., Pan, Y., Liu, D., Li, S., Li, Z., Zhu, F., Zhang, N., Fu, P., and Fang, Y.:
592 Seasonal pattern of ammonium ¹⁵N natural abundance in precipitation at a rural forested site and implications
593 for NH₃ source partitioning, *Environ. Pollut.*, 247, 541-549, <https://doi.org/10.1016/j.envpol.2019.01.023>,
594 2019.

595 Huang, Z., Wang, S., Zheng, J., Yuan, Z., Ye, S., and Kang, D.: Modeling inorganic nitrogen deposition in
596 Guangdong province, China, *Atmos. Environ.*, 109, 147-160,
597 <https://doi.org/10.1016/j.atmosenv.2015.03.014>, 2015.

598 Jiang, H., Li, J., Sun, R., Tian, C., Tang, J., Jiang, B., Liao, Y., Chen, C., and Zhang, G.: Molecular dynamics and
599 light absorption properties of atmospheric dissolved organic matter, *Environ. Sci. Technol.*, 55, 10268-10279,
600 <https://doi.org/10.1021/acs.est.1c01770>, 2021a.

601 Jiang, H., Li, J., Sun, R., Liu, G., Tian, C., Tang, J., Cheng, Z., Zhu, S., Zhong, G., Ding, X., and Zhang, G.:
602 Determining the sources and transport of brown carbon using radionuclide tracers and modeling, *J. Geophys.*
603 *Res.: Atmos.*, 126, e2021JD034616, <https://doi.org/10.1029/2021jd034616>, 2021b.

604 Johnston, J. C. and Thiemens, M. H.: The isotopic composition of tropospheric ozone in three environments, *J.*
605 *Geophys. Res.: Atmos.*, 102, 25395-25404, <https://doi.org/10.1029/97jd02075>, 1997.

606 Kang, Y., Liu, M., Song, Y., Huang, X., Yao, H., Cai, X., Zhang, H., Kang, L., Liu, X., Yan, X., He, H., Zhang,
607 Q., Shao, M., and Zhu, T.: High-resolution ammonia emissions inventories in China from 1980 to 2012,
608 *Atmos. Chem. Phys.*, 16, 2043-2058, <https://doi.org/10.5194/acp-16-2043-2016>, 2016.

609 Kawashima, H. and Kurahashi, T.: Inorganic ion and nitrogen isotopic compositions of atmospheric aerosols at
610 Yurihonjo, Japan: implications for nitrogen sources, *Atmos. Environ.*, 45, 6309-6316,
611 <https://doi.org/10.1016/j.atmosenv.2011.08.057>, 2011.

612 Kundu, S., Kawamura, K., and Lee, M.: Seasonal variation of the concentrations of nitrogenous species and their
613 nitrogen isotopic ratios in aerosols at Gosan, Jeju Island: Implications for atmospheric processing and source
614 changes of aerosols, *J. Geophys. Res.*, 115, <https://doi.org/10.1029/2009jd013323>, 2010.

615 Li, T. and Li, J.: High contribution of anthropogenic combustion sources to atmospheric inorganic reactive
616 nitrogen in south China evidenced by isotopes, Mendeley data [data set],
617 <https://doi.org/10.17632/yck5xy22w2.1>, 2023.

618 Li, X. H. and Wang, S. X.: Particulate and trace gas emissions from open burning of wheat straw and corn stover
619 in China, *Environ. Sci. Technol.*, 41, 6052-6058, <https://doi.org/10.1021/es0705137>, 2007.

620 Liao, B., Wu, D., Chang, Y., Lin, Y., Wang, S., and Li, F.: Characteristics of particulate SO₄²⁻, NO₃⁻, NH₄⁺, and
621 related gaseous pollutants in Guangzhou (in Chinese), *Acta Sci. Circumst.*, 34, 1551-1559,
622 <https://doi.org/10.13671/j.hjkxxb.2014.0218>, 2014.

623 Liu, J., Ding, P., Zong, Z., Li, J., Tian, C., Chen, W., Chang, M., Salazar, G., Shen, C., Cheng, Z., Chen, Y., Wang,
624 X., Szidat, S., and Zhang, G.: Evidence of rural and suburban sources of urban haze formation in China: a
625 case study from the Pearl River Delta region, *J. Geophys. Res.: Atmos.*, 123, 4712-4726,
626 <https://doi.org/10.1029/2017jd027952>, 2018.

627 Liu, T., Wang, X., Wang, B., Ding, X., Deng, W., Lü, S., and Zhang, Y.: Emission factor of ammonia (NH₃) from
628 on-road vehicles in China: tunnel tests in urban Guangzhou, *Environ. Res. Lett.*, 9, 064027,

629 <https://doi.org/10.1088/1748-9326/9/6/064027>, 2014.

630 Liu, Y., Zhang, Y., Lian, C., Yan, C., Wang, Y., Ge, M., He, H., and Kulmala, M.: The promotion effect of nitrous
631 acid on aerosol formation in wintertime in Beijing: the possible contribution of traffic-related emissions,
632 *Atmos. Chem. Phys.*, 20, 13023–13040, <https://doi.org/10.5194/acp-20-13023-2020>, 2020.

633 Liu, Y., Feng, Z., Zheng, F., Bao, X., Liu, P., Ge, Y., Zhao, Y., Jiang, T., Liao, Y., Zhang, Y., Fan, X., Yan, C., Chu,
634 B., Wang, Y., Du, W., Cai, J., Bianchi, F., Petäjä, T., Mu, Y., He, H., and Kulmala, M.: Ammonium nitrate
635 promotes sulfate formation through uptake kinetic regime, *Atmos. Chem. Phys.*, 21, 13269–13286,
636 <https://doi.org/10.5194/acp-21-13269-2021>, 2021.

637 Martinellia, L. A., Camargoa, P. B., Laraa, L. B. L. S., Victoriaa, R. L., and Artaxo, P.: Stable carbon and nitrogen
638 isotopic composition of bulk aerosol particles in a C4 plant landscape of southeast Brazil, *Atmos. Environ.*,
639 36, 2427–2432, [https://doi.org/10.1016/S1352-2310\(01\)00454-X](https://doi.org/10.1016/S1352-2310(01)00454-X), 2002.

640 Meng, W., Zhong, Q., Yun, X., Zhu, X., Huang, T., Shen, H., Chen, Y., Chen, H., Zhou, F., Liu, J., Wang, X., Zeng,
641 E. Y., and Tao, S.: Improvement of a global high-resolution ammonia emission inventory for combustion and
642 industrial sources with new data from the residential and transportation sectors, *Environ. Sci. Technol.*, 51,
643 2821-2829, <https://doi.org/10.1021/acs.est.6b03694>, 2017.

644 Meng, Z., Xu, X., Lin, W., Ge, B., Xie, Y., Song, B., Jia, S., Zhang, R., Peng, W., Wang, Y., Cheng, H., Yang, W.,
645 and Zhao, H.: Role of ambient ammonia in particulate ammonium formation at a rural site in the North China
646 Plain, *Atmos. Chem. Phys.*, 18, 167-184, <https://doi.org/10.5194/acp-18-167-2018>, 2018.

647 Michalski, G., Bhattacharya, S. K., and Girsch, G.: NO_x cycle and the tropospheric ozone isotope anomaly: an
648 experimental investigation, *Atmos. Chem. Phys.*, 14, 4935-4953, <https://doi.org/10.5194/acp-14-4935-2014>,
649 2014.

650 Pan, Y., Tian, S., Liu, D., Fang, Y., Zhu, X., Gao, M., Gao, J., Michalski, G., and Wang, Y.: Isotopic evidence for
651 enhanced fossil fuel sources of aerosol ammonium in the urban atmosphere, *Environ. Pollut.*, 238, 942-947,
652 <https://doi.org/10.1016/j.envpol.2018.03.038>, 2018a.

653 Pan, Y., Tian, S., Liu, D., Fang, Y., Zhu, X., Zhang, Q., Zheng, B., Michalski, G., and Wang, Y.: Fossil fuel
654 combustion-related emissions dominate atmospheric ammonia sources during severe haze episodes:
655 evidence from ¹⁵N-stable isotope in size-resolved aerosol ammonium, *Environ. Sci. Technol.*, 50, 8049-8056,
656 <https://doi.org/10.1021/acs.est.6b00634>, 2016.

657 Pan, Y., Tian, S., Liu, D., Fang, Y., Zhu, X., Gao, M., Wentworth, G. R., Michalski, G., Huang, X., and Wang, Y.:
658 Source Apportionment of Aerosol Ammonium in an Ammonia-Rich Atmosphere: An Isotopic Study of
659 Summer Clean and Hazy Days in Urban Beijing, *J. Geophys. Res.: Atmos.*, 123, 5681-5689,
660 <https://doi.org/10.1029/2017jd028095>, 2018b.

661 Pan, Y., Gu, M., He, Y., Wu, D., Liu, C., Song, L., Tian, S., Lü, X., Sun, Y., Song, T., Walters, W. W., Liu, X.,
662 Martin, N. A., Zhang, Q., Fang, Y., Ferracci, V., and Wang, Y.: Revisiting the concentration observations and
663 source apportionment of atmospheric ammonia, *Adv. Atmos. Sci.*, 37, 933-938,
664 <https://doi.org/10.1007/s00376-020-2111-2>, 2020.

665 Qu, K., Wang, X., Xiao, T., Shen, J., Lin, T., Chen, D., He, L. Y., Huang, X. F., Zeng, L., Lu, K., Ou, Y., and Zhang,
666 Y.: Cross-regional transport of PM_{2.5} nitrate in the Pearl River Delta, China: Contributions and mechanisms,
667 *Sci. Total Environ.*, 753, 142439, <https://doi.org/10.1016/j.scitotenv.2020.142439>, 2021.

668 Savarino, J., Kaiser, J., Morin, S., Sigman, D. M., and Thiemens, M. H.: Nitrogen and oxygen isotopic constraints
669 on the origin of atmospheric nitrate in coastal Antarctica, *Atmos. Chem. Phys.*, 7, 1925–1945,
670 <https://doi.org/10.5194/acp-7-1925-2007>, 2007.

671 Song, W., Liu, X. Y., Hu, C. C., Chen, G. Y., Liu, X. J., Walters, W. W., Michalski, G., and Liu, C. Q.: Important
672 contributions of non-fossil fuel nitrogen oxides emissions, *Nat. Commun.*, 12, 243,

673 <https://doi.org/10.1038/s41467-020-20356-0>, 2021.

674 Song, Y., Dai, W., Wang, X., Cui, M., Su, H., Xie, S., and Zhang, Y.: Identifying dominant sources of respirable
675 suspended particulates in Guangzhou, China, *Environ. Eng. Sci.*, 25, 959-968,
676 <https://doi.org/10.1089/ees.2007.0146>, 2008.

677 Su, T., Li, J., Tian, C., Zong, Z., Chen, D., and Zhang, G.: Source and formation of fine particulate nitrate in South
678 China: Constrained by isotopic modeling and online trace gas analysis, *Atmos. Environ.*, 231,
679 <https://doi.org/10.1016/j.atmosenv.2020.117563>, 2020.

680 Sun, X., Zong, Z., Li, Q., Shi, X., Wang, K., Lu, L., Li, B., Qi, H., and Tian, C.: Assessing the emission sources
681 and reduction potential of atmospheric ammonia at an urban site in Northeast China, *Environ. Res.*, 198,
682 111230, <https://doi.org/10.1016/j.envres.2021.111230>, 2021.

683 Tan, Z., Lu, K., Jiang, M., Su, R., Wang, H., Lou, S., Fu, Q., Zhai, C., Tan, Q., Yue, D., Chen, D., Wang, Z., Xie,
684 S., Zeng, L., and Zhang, Y.: Daytime atmospheric oxidation capacity in four Chinese megacities during the
685 photochemically polluted season: a case study based on box model simulation, *Atmos. Chem. Phys.*, 19,
686 3493–3513, <https://doi.org/10.5194/acp-19-3493-2019>, 2019.

687 Tang, L., Qu, J., Mi, Z., Bo, X., Chang, X., Anadon, L. D., Wang, S., Xue, X., Li, S., Wang, X., and Zhao, X.:
688 Substantial emission reductions from Chinese power plants after the introduction of ultra-low emissions
689 standards, *Nat. Energy*, 4, 929-938, <https://doi.org/10.1038/s41560-019-0468-1>, 2019.

690 Urey, H. C.: The thermodynamic properties of isotopic substances, *J. Chem. Soc.*, 562-581,
691 <https://doi.org/10.1039/jr9470000562>, 1947.

692 Walters, W. W. and Michalski, G.: Theoretical calculation of oxygen equilibrium isotope fractionation factors
693 involving various NO_y molecules, OH, and H₂O and its implications for isotope variations in atmospheric
694 nitrate, *Geochim. Cosmochim. Acta.*, 191, 89–101 <https://doi.org/10.1016/j.gca.2016.06.039>, 2016.

695 Walters, W. W., Simonini, D. S., and Michalski, G.: Nitrogen isotope exchange between NO and NO₂ and its
696 implications for δ¹⁵N variations in tropospheric NO_x and atmospheric nitrate, *Geophys. Res. Lett.*, 43, 440-
697 448, <https://doi.org/10.1002/2015gl066438>, 2016.

698 Walters, W. W., Tharp, B. D., Fang, H., Kozak, B. J., and Michalski, G.: Nitrogen Isotope Composition of
699 Thermally Produced NO_x from Various Fossil-Fuel Combustion Sources, *Environ. Sci. Technol.*, 49, 11363-
700 11371, <https://doi.org/10.1021/acs.est.5b02769>, 2015.

701 Walters, W. W., Song, L., Chai, J., Fang, Y., Colombi, N., and Hastings, M. G.: Characterizing the spatiotemporal
702 nitrogen stable isotopic composition of ammonia in vehicle plumes, *Atmos. Chem. Phys.*, 20, 11551-11567,
703 <https://doi.org/10.5194/acp-20-11551-2020>, 2020.

704 Wang, C., Duan, J., Ren, C., Liu, H., Reis, S., Xu, J., and Gu, B.: Ammonia emissions from croplands decrease
705 with farm size in China, *Environ. Sci. Technol.*, 56, 9915-9923, <https://doi.org/10.1021/acs.est.2c01061>,
706 2022.

707 Wang, T., Xue, L., Brimblecombe, P., Lam, Y. F., Li, L., and Zhang, L.: Ozone pollution in China: a review of
708 concentrations, meteorological influences, chemical precursors, and effects, *Sci. Total Environ.*, 575, 1582-
709 1596, <https://doi.org/10.1016/j.scitotenv.2016.10.081>, 2017.

710 Wang, X., Carmichael, G., Chen, D., Tang, Y., and Wang, T.: Impacts of different emission sources on air quality
711 during March 2001 in the Pearl River Delta (PRD) region, *Atmos. Environ.*, 39, 5227-5241,
712 <https://doi.org/10.1016/j.atmosenv.2005.04.035>, 2005.

713 Wang, X., Wu, Z., Shao, M., Fang, Y., Zhang, L., Chen, F., Chan, P.-w., Fan, Q., Wang, Q., Zhu, S., and Bao, R.:
714 Atmospheric nitrogen deposition to forest and estuary environments in the Pearl River Delta region, southern
715 China, *Tellus B: Chem. Phys. Meteorol.*, 65, <https://doi.org/10.3402/tellusb.v65i0.20480>, 2013.

716 Wedin, D. A. and Tilman, D.: Influence of nitrogen loading and species composition on the carbon balance of

717 grasslands, *Science*, 274, <https://doi.org/10.1126/science.274.5293.1720>, 1996.

718 Wu, L., Ren, H., Wang, P., Chen, J., Fang, Y., Hu, W., Ren, L., Deng, J., Song, Y., Li, J., Sun, Y., Wang, Z., Liu,
719 C.-Q., Ying, Q., and Fu, P.: Aerosol ammonium in the urban boundary layer in Beijing: insights from nitrogen
720 isotope ratios and simulations in summer 2015, *Environ. Sci. Technol. Lett.*, 6, 389-395,
721 <https://doi.org/10.1021/acs.estlett.9b00328>, 2019.

722 Xiang, Y.-K., Dao, X., Gao, M., Lin, Y.-C., Cao, F., Yang, X.-Y., and Zhang, Y.-L.: Nitrogen isotope characteristics
723 and source apportionment of atmospheric ammonium in urban cities during a haze event in Northern China
724 Plain, *Atmos. Environ.*, 269, 118800, <https://doi.org/10.1016/j.atmosenv.2021.118800>, 2022.

725 Xiao, H. W., Wu, J. F., Luo, L., Liu, C., Xie, Y. J., and Xiao, H. Y.: Enhanced biomass burning as a source of
726 aerosol ammonium over cities in central China in autumn, *Environ. Pollut.*, 266, 115278,
727 <https://doi.org/10.1016/j.envpol.2020.115278>, 2020.

728 Xu, Y., Huang, Z., Jia, G., Fan, M., Cheng, L., Chen, L., Shao, M., and Zheng, J.: Regional discrepancies in
729 spatiotemporal variations and driving forces of open crop residue burning emissions in China, *Sci. Total
730 Environ.*, 671, 536-547, <https://doi.org/10.1016/j.scitotenv.2019.03.199>, 2019.

731 Yang, Y., Li, P., He, H., Zhao, X., Datta, A., Ma, W., Zhang, Y., Liu, X., Han, W., Wilson, M. C., and Fang, J.:
732 Long-term changes in soil pH across major forest ecosystems in China, *Geophys. Res. Lett.*, 42, 933-940,
733 <https://doi.org/10.1002/2014gl062575>, 2015.

734 Yu, X., Shen, L., Hou, X., Yuan, L., Pan, Y., An, J., and Yan, S.: High-resolution anthropogenic ammonia emission
735 inventory for the Yangtze River Delta, China, *Chemosphere*, 251, 126342,
736 <https://doi.org/10.1016/j.chemosphere.2020.126342>, 2020.

737 Zhang, Z., Zeng, Y., Zheng, N., Luo, L., Xiao, H., and Xiao, H.: Fossil fuel-related emissions were the major
738 source of NH₃ pollution in urban cities of northern China in the autumn of 2017, *Environ. Pollut.*, 256,
739 113428, <https://doi.org/10.1016/j.envpol.2019.113428>, 2020.

740 Zhang, Z., Zhu, W., Hu, M., Wang, H., Tang, L., Hu, S., Shen, R., Yu, Y., Song, K., Tan, R., Chen, Z., Chen, S.,
741 Canonaco, F., Prevot, A. S. H., and Guo, S.: Secondary organic aerosol formation in China from urban-
742 lifestyle sources: Vehicle exhaust and cooking emission, *Sci. Total Environ.*, 857, 159340,
743 <https://doi.org/10.1016/j.scitotenv.2022.159340>, 2022.

744 Zhao, Y., Tkacik, D. S., May, A. A., Donahue, N. M., and Robinson, A. L.: Mobile sources are still an important
745 source of secondary organic aerosol and fine particulate matter in the los angeles region, *Environ. Sci.
746 Technol.*, 56, 15328-15336, <https://doi.org/10.1021/acs.est.2c03317>, 2022a.

747 Zhao, Y., Xi, M., Zhang, Q., Dong, Z., Ma, M., Zhou, K., Xu, W., Xing, J., Zheng, B., Wen, Z., Liu, X., Nielsen,
748 C. P., Liu, Y., Pan, Y., and Zhang, L.: Decline in bulk deposition of air pollutants in China lags behind
749 reductions in emissions, *Nat. Geosci.*, 15, 190-195, <https://doi.org/10.1038/s41561-022-00899-1>, 2022b.

750 Zheng, L., Chen, W., Jia, S., Wu, L., Zhong, B., Liao, W., Chang, M., Wang, W., and Wang, X.: Temporal and
751 spatial patterns of nitrogen wet deposition in different weather types in the Pearl River Delta (PRD), China,
752 *Sci. Total Environ.*, 740, 139936, <https://doi.org/10.1016/j.scitotenv.2020.139936>, 2020.

753 Zhu, J., He, N., Wang, Q., Yuan, G., Wen, D., Yu, G., and Jia, Y.: The composition, spatial patterns, and influencing
754 factors of atmospheric wet nitrogen deposition in Chinese terrestrial ecosystems, *Sci. Total Environ.*, 511,
755 777-785, <https://doi.org/10.1016/j.scitotenv.2014.12.038>, 2015.

756 Zong, Z., Shi, X., Sun, Z., Tian, C., Li, J., Fang, Y., Gao, H., and Zhang, G.: Nitrogen isotopic composition of
757 NO_x from residential biomass burning and coal combustion in North China, *Environ. Pollut.*, 304, 119238,
758 <https://doi.org/10.1016/j.envpol.2022.119238>, 2022.

759 Zong, Z., Tan, Y., Wang, X., Tian, C., Li, J., Fang, Y., Chen, Y., Cui, S., and Zhang, G.: Dual-modelling-based
760 source apportionment of NO_x in five Chinese megacities: providing the isotopic footprint from 2013 to 2014,

761 Environ. Int., 137, 105592, <https://doi.org/10.1016/j.envint.2020.105592>, 2020.
762 Zong, Z., Wang, X., Tian, C., Chen, Y., Fang, Y., Zhang, F., Li, C., Sun, J., Li, J., and Zhang, G.: First assessment
763 of NO_x sources at a regional background site in North China using isotopic analysis linked with modeling,
764 Environ. Sci. Technol., 51, 5923-5931, <https://doi.org/10.1021/acs.est.6b06316>, 2017.
765